Boundary Value Problems
a SpringerOpen Journal

RESEARCH Open Access

Numerical analysis of unsteady MHD flow near a stagnation point of a two-dimensional porous body with heat and mass transfer, thermal radiation, and chemical reaction

Stanford Shateyi[1*] and Gerald Tendayi Marewo[2]

*Correspondence:
stanford.shateyi@univen.ac.za
[1]Department of Mathematics, University of Venda, P Bag X5050, Thohoyandou, 0950, South Africa
Full list of author information is available at the end of the article

Abstract

The problem of unsteady MHD flow near a stagnation point of a two-dimensional porous body with heat and mass transfer in the presence of thermal radiation and chemical reaction has been numerically investigated. Using a similarity transformation, the governing time-dependent boundary layer equations for the momentum, heat and mass transfer were reduced to a set of ordinary differential equations. This set of ordinary equations were then solved using the spectral local linearization method together with the successive relaxation method. The study made among others the observation that the local Sherwood number increases with increasing values of the unsteadiness parameter and the Schmidt number. The fluid temperature was found to be significantly reduced by increasing values of the Prandtl number and the thermal radiation parameter. The velocity profiles were found to be reduced by increasing values of the chemical reaction and the Schmidt number as well as by the magnetic parameter.

1 Introduction

Uniform fluid flow over bodies of various geometries has been considered by many researchers over the years due to their numerous applications in industry and engineering. Due to complexity and non-linearity of the modeling governing equations exact solutions are difficulty to obtain. To that end, many researchers have employed different analytical and numerical methods. In recent years, the study of stagnation flow has gained tremendous research interest. Stagnation flow is the fluid motion near the stagnation point. The fluid pressure, and the rates of heat and mass transfer are highest in the stagnation area. A flow can be stagnated by a solid wall or a free stagnation point or a line can exist in the interior of the fluid domain. The study of stagnation point flow was pioneered by Hiemenz in 1911 [1]. Wang [2] investigated the stagnation flow toward a shrinking sheet and found that the convective heat transfer decreases with the shrinking rate due to an increase in the boundary layer thickness. Motsa *et al.* [3] studied the Maxwell fluid for two-dimensional stagnation flow toward a shrinking sheet. Shateyi and Makinde [4] investigated the steady stagnation point flow and heat transfer of an electrically conducting incompressible viscous fluid with convective boundary conditions.

The study of heat generation or absorption in moving fluids is of great importance in problems dealing with chemical reactions and those concerned with dissociating fluids. Heat generation effects may alter the temperature distribution and consequently, the particle deposition rate in nuclear reactors, electronic chips. Chamkha and Ahmed [5] studied the problem of MHD heat and mass transfer by mixed convection in the forward stagnation region of rotating sphere in the presence of heat generation and chemical reaction effects. Bararnia *et al.* [6] investigated analytically the problem of MHD natural convectional flow of a heat generation fluid in a porous medium.

Fluid flows with chemical reaction have key importance in many processes such as drying evaporation at the surface of a water body, energy transfer in a wet cooling electric power, food processing, groves of fruit trees, *etc*. The molecular diffusion of species in the presence of a chemical reaction within or at the boundary layer always exists during several practical diffusive operations. Several researchers have studied flows with chemical reaction reactions. Pal and Talukdar [7] presented the combined effects of Joule heating and a chemical reaction on unsteady MHD mixed convection with viscous dissipation over a vertical plate in the presence of a porous medium and thermal radiation. Hayat *et al.* [8] examined the mass transfer effect on unsteady three-dimensional flow of a coupled stress fluid over a stretching surface with chemical reaction. Najib *et al.* [9] investigated the stagnation point flow and mass transfer with a chemical reaction past a stretching shrinking cylinder.

Unsteady mixed convection flows do not necessarily possess similarity solutions in many practical applications. The unsteadiness and non-similarity in such flows may be due to the free stream velocity or due to the curvature of the body or due to the surface mass transfer or even possibly due to all these effects. Many investigators have confined their studies to either steady non-similar flows or to unsteady semi-similar flows because of the mathematical difficulties involved in obtaining non-similar solutions for such problems. Patil *et al.* [10] numerically studied the combined effects of thermal radiation and Newtonian heating on unsteady mixed convection flow along a semi-infinite vertical plate. Admon *et al.* [11] studied the behavior of unsteady free convection of a viscous and incompressible fluid in the stagnation point region of a heated three-dimensional body considering the temperature-dependent internal heat generation. Ahmad and Nazar [12] investigated the unsteady MHD mixed convection boundary layer flow of a viscoelastic fluid near the stagnation point for a vertical surface. Chamkha and Ahmed [13] investigated the effects of heat generation/absorption and chemical reaction on unsteady MHD flow heat and mass transfer near a stagnation point of three-dimensional porous body in the presence of a uniform magnetic field.

The effect of radiation is important in many non-isothermal situations. If the entire system involving the polymer extrusion process is placed in a thermally controlled environment, then radiation could become very important. Understanding radiation heat transfer in the system can lead to a desired product with a sought characteristic. Mahmoud [14] considered the effects of variable thermal radiation on the flow and heat transfer of an electrically conducting micropolar fluid over a continuously stretching surface with varying temperature in the presence of a magnetic field. Recently, Rashidi *et al.* [15] found the analytic solutions using the homotopy analysis method for velocity, temperature, and concentration distributions to study the steady magneto hydrodynamic fluid flow over a stretching sheet in the presence of buoyancy forces and thermal radiation. Hassan and

Rashidi [16] presented an analytical solution for three-dimensional steady flow of a condensation film on an inclined rotating disk by the optical homotopy analysis method. Basiri Parsa *et al.* [17] applied the semi-numerical techniques known as the optimal analysis method (HAM) and the Differential Transform Method (DTM) to study the magneto-hemodynamic laminar viscous flow of a conducting physiological fluid in a semi-porous channel under a transverse magnetic field. Recently Khan *et al.* [18] studied the numerical simulation for unsteady MHD flow and heat transfer of a couple stress fluid over a rotating disk.

The present study aims to investigate the combined effects of thermal radiation, heat generation, viscous dissipation, and chemical reaction on an unsteady mixed convection flow near a stagnation point of two-dimensional porous body. The unsteadiness is induced due to the time-dependent moving plate velocity as well as by the free stream velocity. The paper seeks to compare the performance of two recently developed methods, namely the spectral local linearization method (SLLM) and the spectral relaxation method (SRM). The results generated from these two methods are also validated against the Matlab *bvp*4*c* routine technique.

2 Mathematical formulation

We consider unsteady laminar incompressible boundary layer flow of a viscous electrically conducting fluid at a two-dimensional stagnation point with magnetic field, thermal radiation, heat generation/absorption and suction/injection effects. It is assumed that near the stagnation point the free stream temperature is constant and a uniform transverse magnetic field is applied normal to the body surface. The fluid properties are assumed to be constant and a uniform chemical reaction is taking place within the flow. Following Eswara and Nath [19], the velocity components of the inviscid flow over the two-dimensional body surface are given by

$$u_e(x,t) = \frac{ax}{(1-\lambda\tau)}, \qquad v_e(x,t) = \frac{by}{(1-\lambda\tau)}. \tag{1}$$

We also assume that near the stagnation point, the free stream temperature and concentration are constant. We note that for $T_w > T_\infty$ and/or $C_w > C_\infty$ the buoyancy forces, will aid the flow. On the other hand, for $T_w < T_\infty$ and/or $C_w < C_\infty$, the resulting buoyancy force will oppose the forced flow. Under these assumptions as well as the Boussinesq approximation, and following Chamkha and Ahmed [13], the governing equations for the current study are given by

$$\frac{\partial u}{\partial x} + \frac{\partial v}{\partial y} = 0, \tag{2}$$

$$\frac{\partial u}{\partial t} + u\frac{\partial u}{\partial x} + v\frac{\partial u}{\partial y} = \frac{\partial u_e}{\partial t} + u_e\frac{\partial u_e}{\partial x} + \nu\frac{\partial^2 u}{\partial y^2} - \frac{\sigma B_0^2}{\rho}(u-u_e) + \left[g\beta(T-T_\infty) + g\beta_c(C-C_\infty)\right]\frac{x}{l}, \tag{3}$$

$$\frac{\partial T}{\partial t} + u\frac{\partial T}{\partial x} + v\frac{\partial T}{\partial y} = \frac{k}{\rho c_p}\frac{\partial^2 T}{\partial y^2} + \frac{\mu}{\rho c_p}\left(\frac{\partial u}{\partial y}\right)^2 - \frac{1}{\rho c_p}\frac{\partial q_r}{\partial y} \pm \frac{Q_0}{\rho c_p}(T-T_\infty), \tag{4}$$

$$\frac{\partial T}{\partial t} + u\frac{\partial C}{\partial x} + v\frac{\partial C}{\partial y} = D\frac{\partial^2 C}{\partial y^2} - k_r(C-C_\infty). \tag{5}$$

The initial and boundary conditions are

$$\begin{aligned}
&t = 0 : u(x,y,t) = u_i(x,y), \qquad v(x,y) = v_i(x,y), \qquad T(x,y,t) = T_i(x,y),\\
&C(x,y,t) = C_i(x,y),\\
&t > 0 : u(x,y,t) = 0, \qquad v(x,y,t) = V_w, \qquad T(x,y,t) = T_w,\\
&C(x,y,t) = C_w, \quad \text{at } y = 0,\\
&t > 0 : u = u_e(x,y,t), \qquad v = v_e(x,y,t), \qquad T(x,y,t) = T_\infty,\\
&C(x,y,t) = C_\infty, \quad \text{as } y \to \infty.
\end{aligned} \tag{6}$$

3 Similarity analysis

We assume that the velocity varies inversely as a linear function of time making it possible to transform equations (2)-(5) into a set of self-similar equations.

Applying the dimensionless quantities

$$\begin{aligned}
&\eta = \left(\frac{a}{\nu(1-\lambda\tau)}\right)^{\frac{1}{2}} y, \qquad \tau = at, \qquad u = \frac{ax}{(1-\lambda\tau)} f'(\eta),\\
&v = -\left(\frac{a\nu}{(1-\lambda\tau)}\right)^{\frac{1}{2}} f(\eta), \qquad \theta(\eta) = \frac{T - T_\infty}{T_w - T_\infty}, \qquad \phi(\eta) = \frac{C - C_\infty}{C_w - C_\infty}
\end{aligned} \tag{7}$$

to (2)-(5) yields the following similarity equations:

$$f''' + ff'' - \frac{\lambda\eta}{2} f'' - \lambda f' - f'^2 - M\left(f' - 1\right) + \lambda_1\theta + \lambda_2\phi + (\lambda + 1) = 0, \tag{8}$$

$$\left(\frac{4 + 3R}{3PrR}\right)\theta'' + \left(f - \frac{\lambda\eta}{2}\right)\theta' + \delta\theta + Ecf''^2 = 0, \tag{9}$$

$$\frac{1}{Sc}\phi'' + \left(f - \frac{\lambda\eta}{2}\right)\phi' - \gamma\phi = 0, \tag{10}$$

where $M = \sigma B_0^2/\rho a$ is the magnetic field parameter, λ is the unsteadiness parameter, $\lambda_1 = Gr/Re_l^2$, $\lambda_2 = Gr_c/Re_l^2$ are the buoyancy parameters, $Pr = \mu c_p/k$ is the Prandtl number, $Gr = g\beta l^3(T_w - T_\infty)/\nu^2$ is the Grashof number, $Gr_c = g\beta l^3(C_w - C_\infty)/\nu^2$ is the modified Grashof number, $Re_l = al^2/\nu$ is the Reynolds number, $\delta = Q_0/\rho c_p a$ is the heat generation/absorption parameter, $E_c = \nu a^2 x^2/c_p(1-\lambda\tau)(T_w - T_\infty)$, $Sc = \nu/D$ is the Schmidt number, $\gamma = \frac{k_r}{a}(1-\lambda\tau)$.

The transformed boundary conditions (6) become

$$f(0) = f_w, \qquad f'(0) = 0, \qquad \theta(0) = 1, \qquad \phi(0) = 1, \tag{11}$$

$$f' \to 1, \qquad \theta \to 0, \qquad \phi \to 0 \quad \text{as } \eta \to \infty, \tag{12}$$

where $f_w = -V_w((1-\lambda\tau)/a\nu)^{\frac{1}{2}}$ is the suction/injection parameter.

4 Methods of solution

4.1 Spectral local linearization method (SLLM)

4.1.1 Basic idea

Let $r = 0, 1, 2, \ldots$. Suppose that $r + 1$ iterations of the SLLM have been used to solve a given a system of differential equations such as equations (8)-(10). Also, suppose that each equation can be written in the form

$$L|_{r+1} + N|_{r+1} = H, \tag{13}$$

where L and N are the linear and non-linear components, respectively, and H is a given function of η. Let $\mathbf{w}$ be the n-tuple consisting of independent variable z and its derivatives. If we assume that N is a function of $\mathbf{w}$ only, then equation (13) may be replaced with the linearized form

$$L|_{r+1} + N|_r + \nabla N|_r \cdot (\mathbf{w}_{r+1} - \mathbf{w}_r) = H, \tag{14}$$

which shall be solved using the Chebyshev Spectral Collocation Method [20]. We chose this method due to its ease of implementation and relatively high rate of convergence.

4.1.2 Application

Upon using the transformation $p = f'$, equations (8) and (9) become

$$p'' + fp' - \lambda\frac{\eta}{2}p' - \lambda p - p^2 - M(p-1) + \lambda_1\theta + \lambda_2\phi + (\lambda + 1) = 0, \tag{15}$$

$$\left(\frac{4+3R}{3PrR}\right)\theta'' + \left(f - \lambda\frac{\eta}{2}\right)\theta' + \delta\theta + Ecp'^2 = 0, \tag{16}$$

but equation (10) remains unchanged.

Equation (15) may be written in the same form as equation (13) with

$$L = p'' - \lambda\frac{\eta}{2}p' - (\lambda + M)p + \lambda_1\theta + \lambda_2\phi + (\lambda + 1), \tag{17}$$

$$N(p, p') = fp' - p^2 \quad \text{and} \quad H = -M. \tag{18}$$

The corresponding linearized form (14) is

$$L|_{r+1} + \frac{\partial N}{\partial p}\Big|_r p_{r+1} + \frac{\partial N}{\partial p'}\Big|_r p'_{r+1} = H + \frac{\partial N}{\partial p}\Big|_r p_r + \frac{\partial N}{\partial p'}\Big|_r p'_r - N|_r, \tag{19}$$

which upon making use of equations (17) and (18), and simplifying becomes

$$\begin{aligned} &p''_{r+1} - \lambda\frac{\eta}{2}p'_{r+1} - (\lambda + M)p_{r+1} + \lambda_1\theta_{r+1} + \lambda_2\phi_{r+1} - 2p_rp_{r+1} + f_rp'_{r+1} \\ &\quad = -M - p_r^2 - (\lambda + 1). \end{aligned} \tag{20}$$

Similarly, equations (16) and (10) yield

$$\left(\frac{4+3R}{3PrR}\right)\theta''_{r+1} - \lambda\frac{\eta}{2}\theta'_{r+1} + \delta\theta_{r+1} + f_r\theta'_{r+1} = -Ecp'^2_r, \tag{21}$$

$$\frac{1}{Sc}\phi''_{r+1} - \lambda\frac{\eta}{2}\phi'_{r+1} - \gamma\phi_{r+1} + f_r\phi'_{r+1} = 0. \tag{22}$$

Before we solve iterative equations (20), (21), and (22) for each $r = 0, 1, 2, \ldots$, we take the following preliminary steps.

1. The infinite interval $[0, \infty)$ on the η axis is replaced by the finite interval $[0, L_1]$, where L_1 is sufficiently large.
2. The truncated problem domain $[0, L_1]$ on the η axis is mapped onto the computational domain $[-1, 1]$ on the ξ axis.
3. The computational domain is partitioned using the Chebyshev collocation points $\xi_0, \xi_1, \ldots, \xi_N$, where $-1 = \xi_N < \xi_{N-1} < \cdots < \xi_0 = 1$.

For a more detailed explanation of these steps, see for example [21] and [22].

Equations (20) through (22) are subject to the boundary conditions

$$p_{r+1}(\xi_N) = 0, \qquad p_{r+1}(\xi_0) = 1, \tag{23}$$

$$\theta_{r+1}(\xi_N) = 1, \qquad \theta_{r+1}(\xi_0) = 0, \tag{24}$$

$$\phi_{r+1}(\xi_N) = 1, \qquad \phi_{r+1}(\xi_0) = 0, \tag{25}$$

respectively. Applying Chebyshev differentiation [20], as done in *e.g.* [22], transforms equations (20)-(22) and (23)-(25), by the transformation $f' = p$ with boundary condition $f(0) = f_w$, to the discrete system

$$A_1\Phi_{r+1} = B_1, \qquad \phi_{r+1}(\xi_N) = 1, \qquad \phi_{r+1}(\xi_0) = 0, \tag{26}$$

$$A_2\Theta_{r+1} = B_2, \qquad \theta_{r+1}(\xi_N) = 1, \qquad \theta_{r+1}(\xi_0) = 0, \tag{27}$$

$$A_3\mathbf{p}_{r+1} = B_3, \qquad p_{r+1}(\xi_N) = 0, \qquad p_{r+1}(\xi_0) = 1, \tag{28}$$

$$A_4\mathbf{f}_{r+1} = B_4, \qquad f_{r+1}(\xi_N) = f_w, \tag{29}$$

where

$$A_1 = \frac{1}{Sc}D^2 + \left(-\frac{\lambda}{2}\eta I + \operatorname{diag}\{\mathbf{f}_r\}\right)D - \gamma I, \qquad B_1 = \mathbf{0}, \tag{30}$$

$$A_2 = \left(\frac{4+3R}{3PrR}\right)D^2 + \left(-\frac{\lambda}{2}\eta I + \operatorname{diag}\{\mathbf{f}_r\}\right)D + \delta I, \qquad B_2 = -Ec\mathbf{p}_r'^2, \tag{31}$$

$$A_3 = D^2 + \left(-\frac{\lambda}{2}\eta I + \operatorname{diag}\{\mathbf{f}_r\}\right)D - (\lambda + M)I - 2\operatorname{diag}\{\mathbf{p}_r\}, \tag{32}$$

$$B_3 = -M - (\lambda + 1) - \mathbf{p}_r^2 - [\lambda_1\Theta_{r+1} + \lambda_2\Phi_{r+1}], \tag{33}$$

$$A_4 = D, \qquad B_4 = \mathbf{p}_{r+1}. \tag{34}$$

The solution of each linear system in equations (26)-(28) is preceded by including the corresponding boundary conditions. We do this in the same manner as [21]. For example, the linear system in equation (26) becomes

$$\left(\begin{array}{c|c|c} 1 & 0 \cdots 0 & \\ \hline & A_1 & \\ \hline 0 \cdots 0 & & 1 \end{array}\right)\left(\begin{array}{c} \phi_{r+1}(\xi_0) \\ \hline \vdots \\ \hline \phi_{r+1}(\xi_N) \end{array}\right) = \left(\begin{array}{c} 0 \\ \hline B_1 \\ \hline 1 \end{array}\right).$$

Equations (27) and (28) are modified in a similar manner, while equation (29) becomes

$$\left(\begin{array}{c} A_4 \\ \hline 0 \quad \cdots \quad 0 \quad 1 \end{array}\right)\left(\begin{array}{c} f_{r+1}(\xi_0) \\ \vdots \\ \hline f_{r+1}(\xi_N) \end{array}\right) = \left(\begin{array}{c} B_4 \\ \hline f_w \end{array}\right).$$

The SLLM is driven by initial approximations

$$f_0(\eta) = \eta + e^{-\eta} + f_w - 1,$$
$$p_0(\eta) = 1 - e^{-\eta},$$
$$\theta_0(\eta) = \phi_0(\eta) = e^{-\eta},$$

which are chosen so that they satisfy boundary conditions (11) and (12). Successive application of the SLLM generates approximations f_{r+1}, p_{r+1}, θ_{r+1}, ϕ_{r+1} for each $r = 0, 1, 2, \ldots$.

4.2 Successive relaxation method (SRM)

Just like the SLLM, the SRM also makes use of the transformation $p = f'$ on the governing equations (8)-(10). Hence, we begin with the transformed equations (15) and (16), and equation (10), which is invariant under this transformation.

As done in [4] and [21], we proceed in a manner similar to the Gauss-Seidel method for solving a linear system. Consequently, we replace the transformation $p = f'$ and equations (15), (16), and (10) with the iterative equations

$$f'_{r+1} = p_r, \tag{35}$$
$$p''_{r+1} + \left(f_{r+1} - \lambda\frac{\eta}{2}\right)p'_{r+1} - (\lambda + M)p_{r+1} = p_r^2 - M - (\lambda_1\theta_r + \lambda_2\phi_r) - (\lambda + 1), \tag{36}$$
$$\left(\frac{4 + 3R}{3PrR}\right)\theta''_{r+1} + \left(f_{r+1} - \lambda\frac{\eta}{2}\right)\theta'_{r+1} + \delta\theta_{r+1} + Ecp'^2_{r+1} = 0, \tag{37}$$
$$\frac{1}{Sc}\phi''_{r+1} + \left(f_{r+1} - \lambda\frac{\eta}{2}\right)\phi'_{r+1} - \gamma\phi_{r+1} = 0, \tag{38}$$

subject to boundary condition

$$f_{r+1}(\xi_N) = f_w, \tag{39}$$

and boundary conditions (23)-(25), respectively.

Just like with the SLLM, we use Chebyshev differentiation to replace equations (35) through (38) with the discrete form

$$A_1\mathbf{f}_{r+1} = B_1, \qquad f_{r+1}(\xi_N) = f_w, \tag{40}$$
$$A_2\mathbf{p}_{r+1} = B_2, \qquad p_{r+1}(\xi_N) = 0, \qquad p_{r+1}(\xi_0) = 1, \tag{41}$$
$$A_3\Theta_{r+1} = B_3, \qquad \theta_{r+1}(\xi_N) = 1, \qquad \theta_{r+1}(\xi_0) = 0, \tag{42}$$
$$A_4\Phi_{r+1} = B_4, \qquad \phi_{r+1}(\xi_N) = 1, \qquad \phi_{r+1}(\xi_0) = 0, \tag{43}$$

where

$$A_1 = D, \qquad B_1 = \mathbf{p}_r, \tag{44}$$

$$\begin{aligned} A_2 &= D^2 + \operatorname{diag}\{\mathbf{f}_{r+1}\}D - \lambda\frac{\eta}{2}D - (\lambda + M)I, \\ B_2 &= \mathbf{p}_r^2 - M - (\lambda_1\Theta_r + \lambda_2\Phi_r) - (\lambda + 1), \end{aligned} \tag{45}$$

$$A_3 = \left(\frac{4+3R}{3PrR}\right)D^2 + \operatorname{diag}\{\mathbf{f}_{r+1}\}D - \lambda\frac{\eta}{2}D + \delta I, \qquad B_3 = -Ec\mathbf{p}'^{\,2}_{r+1}, \tag{46}$$

$$A_4 = \frac{1}{Sc}D^2 + \operatorname{diag}\{\mathbf{f}_{r+1}\}D - \lambda\frac{\eta}{2}D - \gamma I, \qquad B_4 = \mathbf{0}. \tag{47}$$

Just like with the SLLM, the following steps are done in a similar manner for the SRM:

- For each linear system in equations (40)-(43), include the corresponding boundary conditions.
- Choose suitable initial approximations f_0, p_0, θ_0, ϕ_0 required by the SRM to generate subsequent approximations f_{r+1}, p_{r+1}, θ_{r+1}, ϕ_{r+1} for each $r = 0, 1, 2, \ldots$.

5 Results and discussion

In this section we present a comprehensive numerical parametric study is conducted and the results are reported graphically and in tabular form. Numerical simulations were carried out to obtain approximate numerical values of the quantities of engineering interest. The quantities are the surface shear stress $f''(0)$, surface heat transfer $\theta'(0)$, and surface mass transfer $\phi'(0)$. In both the SLLM and the SRM numerical simulations, a finite computational value of $\eta_\infty = 30$ was chosen in the η direction. This was reached through numerical experimentations. This value was found to give accurate results for all the governing physical parameters and beyond the value, the results did not change within prescribed significant accuracy. The number of collocation points used in both SLLM and SRM was $Nx = 50$ in all the cases considered in this investigation. We set our tolerance level to be $\varepsilon = 10^{-8}$ which we regard to be good enough for any engineering numerical approximation.

We compare the performance of the two methods against each other as well as to the *bvp*4*c* method. Table 1 displays the results generated by the three methods. When varying the magnetic fields strength, it can be clearly observed in the table that, for the current problem, the SLLM is superior to both the SRM and the *bvp*4*c* methods.

The table shows the total computational time needed to generate the results to the desired accuracy. The results displayed in these table are quite interesting. First, it can be clearly seen that the computational run for the SLLM takes far less computer time than both the SRM and the *bvp*4*c* of the three methods, the *bvp*4*c* is the slowest. The SLLM converges much faster than the other two methods. For some default values of the parameters, the SLLM takes a maximum of nine iterations before convergence is achieved, whereas the SRM requires as many as 34 iterations for the same default values. We therefore conclude that the SLLM is the best of the three methods for the current problem. To that end, all the subsequent results displayed on tabular and graphical forms were generated using the SLLM. Table 2 displays the effect of increasing the magnetic field strength on the surface shear stress, heat, and mass transfer on the surface. We observe in this table that the skin friction is greatly increased as the values of the magnetic parameter increases,

Table 1 Comparison of the SLLM results of $f''(0)$ with those obtained by SRM as well as by *bvp4c* for different values of the magnetic parameter M, with $\lambda = 0.5$; $R = 1$; $Pr = 0.71$; $\lambda_1 = 0.5$; $\lambda_2 = 0.5$; $Ec = 0.1$; $\gamma = 0.1$; $\delta = 0.1$; $fw = 0.5$; $Sc = 0.22$

	SLLM			*SRM*			*bvp4c*	
M	*it*	time (sec)	$f''(0)$	*it*	time (sec)	$f''(0)$	time (sec)	$f''(0)$
1	9	1.37	2.48466051	34	3.74	2.48466051	15.27	2.48466051
3	8	0.74	2.88909949	21	3.32	2.88909949	17.86	2.88909949
5	8	0.96	3.24098431	17	2.81	3.24098431	18.53	3.24098431
10	7	0.82	3.98172655	13	1.76	3.98172655	18.37	3.98172655

Table 2 Effect of the magnetic parameter on $f''(0)$, $-\theta'(0)$, $-\phi'(0)$ with $\lambda = 0.5$; $R = 1$; $Pr = 0.71$; $\lambda_1 = 0.5$; $\lambda_2 = 0.5$; $Ec = 0.1$; $\gamma = 0.1$; $\delta = 0.1$; $fw = 0.5$; $Sc = 0.22$

M	$f''(0)$	$-\theta'(0)$	$-\phi'(0)$
0	2.25937547	0.37888463	0.49382391
2	2.69541174	0.37785044	0.49091212
5	3.24098431	0.37663629	0.48843976

Table 3 Effect of the transpiration parameter f_w on $f''(0)$, $-\theta'(0)$, $-\phi'(0)$ with $\lambda = 0.5$; $R = 1$; $Pr = 0.71$; $\lambda_1 = 0.5$; $\lambda_2 = 0.5$; $Ec = 0.1$; $\gamma = 0.1$; $\delta = 0.1$; $M = 2$; $Sc = 0.22$

f_w	$f''(0)$	$-\theta'(0)$	$-\phi'(0)$
–0.5	2.12463544	0.18753160	0.36279720
0.0	2.39659776	0.27651084	0.42802020
0.5	2.69541174	0.37785044	0.49091212
1.0	3.01855731	0.48914126	0.56352188

Table 4 The influence of the heat generation/absorption parameter δ on $f''(0)$, $-\theta'(0)$, $-\phi'(0)$ with $\lambda = 0.5$; $R = 1$; $Pr = 0.71$; $\lambda_1 = 0.5$; $\lambda_2 = 0.5$; $Ec = 0.1$; $\gamma = 0.1$; $M = 2$; $fw = 0.5$; $Sc = 0.22$

δ	$f''(0)$	$-\theta'(0)$	$-\phi'(0)$
–0.5	2.67966177	0.56304464	0.48999569
0.0	2.71117974	0.41294180	0.49072523
0.5	2.74660998	0.13156107	0.49424792

while both the heat and the mass transfer on the surface are reduced. Physically, the application of a magnetic field in the normal direction to the flow produces a drag force which tend to retard the fluid flow velocity, thus increasing the temperature and mass distribution within the fluid flow. In Table 3, we display the influence of the transpiration parameter fw on the skin friction, the Nusselt number and the Sherwood number. Blowing fluid, with $fw < 0$, into the system reduces these three physical quantities whereas sucking fluid, $fw > 0$, out of the system increases the three physical quantities under consideration.

Generating heat within the flow system significantly affects the heat transfer on the surface. The Nusselt number is greatly reduced as heat is generated, but the skin friction as well as the Sherwood number is increased as the heat is generated. These can easily be seen on Table 4.

Table 5 displays the effect of the unsteadiness parameter λ on the shear surface stress, heat transfer on the surface and mass transfer. We consider the accelerating cases only, $\lambda > 0$. Increasing the unsteadiness parameter greatly increases the skin friction but reduces both the heat and the mass transfer on the surface.

Table 5 The influence of the unsteadiness parameter λ on $f''(0)$, $-\theta'(0)$, $-\phi'(0)$ with $\delta = 0.1$; $R = 1$; $Pr = 0.71$; $\lambda_1 = 0.5$; $\lambda_2 = 0.5$; $Ec = 0.1$; $\gamma = 0.1$; $M = 2$; $fw = 0.5$; $Sc = 0.22$

λ	$f''(0)$	$-\theta'(0)$	$-\phi'(0)$
0	2.61770412	0.44070738	0.52781664
0.5	2.69541174	0.37785044	0.49091212
1.0	2.77234572	0.30219385	0.45252502
1.5	2.84976599	0.20022768	0.41157441

Table 6 The effect of the temperature buoyancy parameter λ_1 on $f''(0)$, $-\theta'(0)$, $-\phi'(0)$ with $\delta = 0.1$; $R = 1$; $Pr = 0.71$; $\lambda = 0.5$; $\lambda_2 = 0.5$; $Ec = 0.1$; $\gamma = 0.1$; $M = 2$; $fw = 0.5$; $Sc = 0.22$

λ_1	$f''(0)$	$-\theta'(0)$	$-\phi'(0)$
−0.5	2.23773235	0.36058187	0.52781664
0.0	2.46917284	0.36975021	0.49091212
0.5	2.69541174	0.37785044	0.45252502

Table 7 The influence of the Eckert number Ec on $f''(0)$, $-\theta'(0)$, $-\phi'(0)$ with $\delta = 0.1$; $R = 1$; $Pr = 0.71$; $\lambda = 0.5$; $\lambda_1 = 0.5$; $\lambda_2 = 0.5$; $\gamma = 0.1$; $M = 2$; $fw = 0.5$; $Sc = 0.22$

Ec	$f''(0)$	$-\theta'(0)$	$-\phi'(0)$
0	2.69467396	0.40027022	0.49088572
0.1	2.70208324	0.17491583	0.49115055
0.5	2.70956330	0.05303825	0.49173820

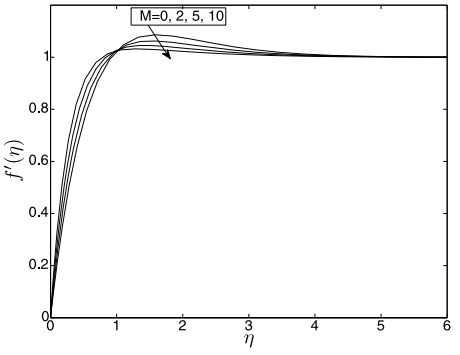

Figure 1 Graph of the SLLM solutions for the horizontal velocity for different values of M, with $\lambda = 0.5$; $R = 1$; $Pr = 0.71$; $\lambda_1 = 0.5$; $\lambda_2 = 0.5$; $Ec = 0.1$; $\gamma = 0.1$; $\delta = 0.1$; $fw = 0.5$; $Sc = 0.22$.

Table 6 displays the effect of temperature buoyancy parameter λ_1 on the skin friction, Nusselt number and Sherwood number. As expected, buoyancy has significant effect on the flow properties. The skin friction increases as the values of the buoyancy parameters are increased. Also the rate of mass transfer at the surface increases as the buoyancy parameters increase, however, the rate of heat transfer decreases with increasing values of the buoyancy parameters.

In Table 7 we show the influence of the Eckert number on the skin friction, and the rates of heat and mass transfer. Evidently, the rate of heat transfer is greatly reduced as the values of the Eckert number increases. Figure 1 displays the effect of the magnetic field strength on the velocity profiles. As expected, the velocity rapidly increases from zero toward the free stream velocity value. We also observe that within the region $\eta < 1$, the velocity increases as the magnetic parameter values increase. However, for $\eta > 1$, the velocity profiles are reduced with increasing values of the magnetic parameter. Application of a transverse magnetic field in the direction normal to the flow direction produces a

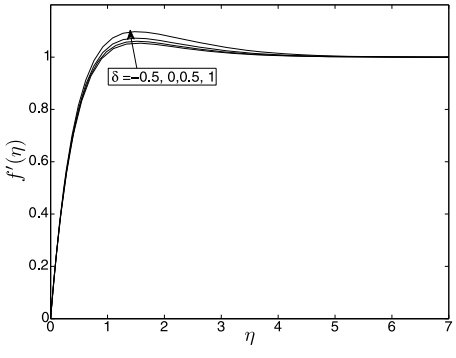

Figure 2 Graph of the SLLM solutions for the horizontal velocity for different values of δ, with $\lambda = 0.5$; $R = 1$; $Pr = 0.71$; $\lambda_1 = 0.5$; $\lambda_2 = 0.5$; $Ec = 0.1$; $\gamma = 0.1$; $M = 0.5$; $fw = 0.5$; $Sc = 0.22$.

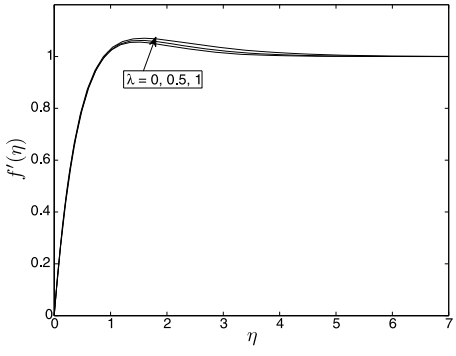

Figure 3 Graph of the SLLM solutions for the horizontal velocity for different values of λ, with $f_w = 0.5$; $R = 1$; $Pr = 0.71$; $\lambda_1 = 0.5$; $\lambda_2 = 0.5$; $Ec = 0.1$; $\gamma = 0.1$; $M = 0.5$; $fw = 0.5$; $Sc = 0.22$.

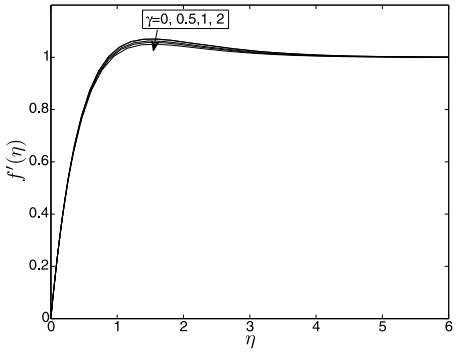

Figure 4 The influence of the chemical reaction parameter on the horizontal velocity for with $\lambda = 0.5$; $R = 1$; $Pr = 0.71$; $\lambda_1 = 0.5$; $\lambda_2 = 0.5$; $Ec = 0.1$; $\delta = 0.1$; $M = 0.5$; $\delta = 0.1$; $Sc = 0.22$.

drag-like force called the Lorentz force. This force tends to cause deceleration in the fluid motion and, therefore, the velocity profiles decrease with increasing values of the magnetic field strength field parameter.

In Figure 2 we display the influence of the heat generation parameter on the velocity distribution. Heating the fluid lightens the fluid particles reducing the friction within the particle interactions thereby increasing the flow velocity as can be clearly seen on Figure 2.

The effect of the unsteadiness parameter on the velocity profiles is displayed in Figure 3. We observe that near the wall surface, the velocity rapidly increases toward the free stream value. Stretching the sheet accelerates the flow velocity as can be observed in this figure.

In Figure 4, we display the influence of the chemical reaction on the velocity profiles. Though the velocity rapidly increases from zero to the free stream value, we observe in this

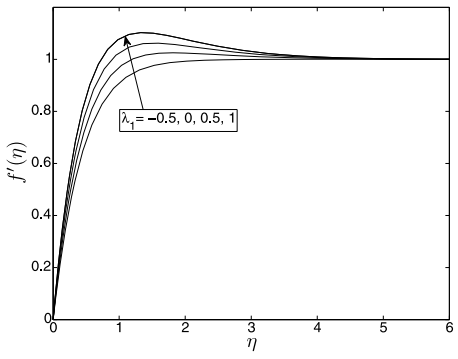

Figure 5 Graph of the SLLM solutions for the horizontal velocity for different values of λ_1, with $f_w = 0.5$; $R = 1$; $Pr = 0.71$; $\lambda = 0.5$; $\lambda_2 = 0.5$; $Ec = 0.1$; $\gamma = 0.1$; $M = 0.5$; $fw = 0.5$; $Sc = 0.22$.

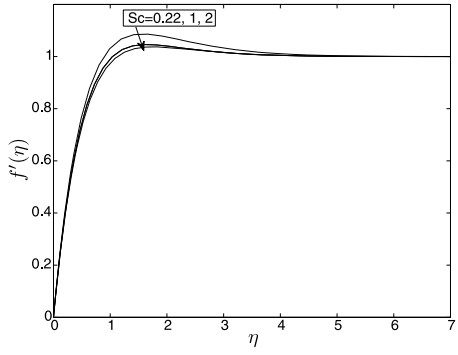

Figure 6 The influence of the chemical reaction parameter on the horizontal velocity for with $\lambda = 0.5$; $R = 1$; $Pr = 0.71$; $\lambda_1 = 0.5$; $\lambda_2 = 0.5$; $Ec = 0.1$; $\delta = 0.1$; $M = 0.5$; $\delta = 0.1$; $Sc = 0.22$.

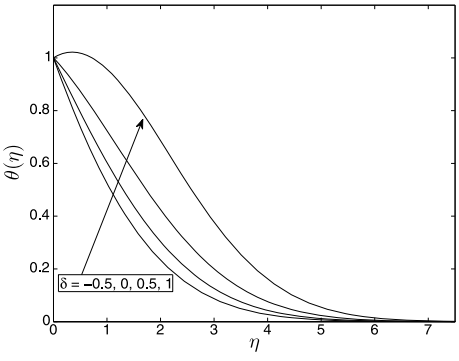

Figure 7 Graph of the SLLM solutions of the temperature profiles for different values of δ, with $\lambda = 0.5$; $R = 1$; $Pr = 0.71$; $\lambda_1 = 0.5$; $\lambda_2 = 0.5$; $Ec = 0.1$; $\gamma = 0.1$; $M = 0.5$; $\delta = 0.1$; $Sc = 0.22$.

figure that in the current study, the chemical reaction parameter has very little influence on the velocity profiles.

Figure 5 shows the effect of the temperature buoyancy parameter λ_1, on the velocity profiles. Increasing the values of the buoyancy parameter leads to the increase of temperature gradient. This in turn cause the increases in the values of the velocity profiles as more forces are added with this increase in buoyancy parameters.

In Figure 6, we display the effect of the Schmidt number on the velocity profiles. Increasing the values of the Schmidt numbers implies that the mass concentration becomes more dense. With all other parameters kept constant, increasing the Schmidt number reduces the flow velocity.

Figure 7 depicts the influence of the heat source/sink on the temperature profiles. The presence of a heat sink leads to the reduction of the temperature distribution. However,

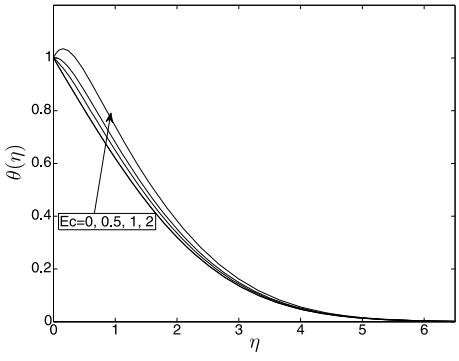

Figure 8 The influence of the Eckert number on the temperature distribution with $\lambda = 0.5$; $R = 1$; $Pr = 0.71$; $\lambda_1 = 0.5$; $\lambda_2 = 0.5$; $Ec = 0.1$; $\delta = 0.1$; $M = 0.5$; $\delta = 0.1$; $Sc = 0.22$.

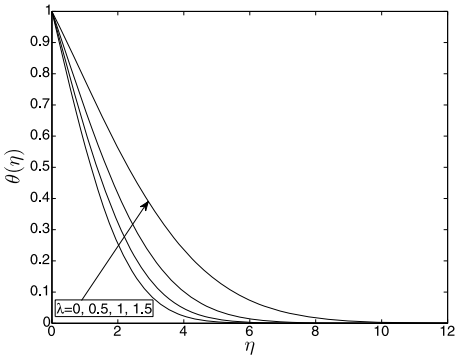

Figure 9 The influence of the unsteadiness number on the temperature distribution with $Ec = 0.1$; $R = 1$; $Pr = 0.71$; $\lambda_1 = 0.5$; $\lambda_2 = 0.5$; $Ec = 0.1$; $\delta = 0.1$; $M = 0.5$; $\delta = 0.1$; $Sc = 0.22$.

the presence of the heat source causes great enhancement of the temperature distribution. Therefore heating the fluid flow enhances heat transfer within the fluid flow.

In Figure 8, we display the influence of the Eckert number on the temperature distribution. Increasing the Eckert number allows energy to be stored in the fluid region as a result of dissipation due to viscosity and elastic deformation thus generating heat due to frictional heating. This then causes the temperature within the fluid flow to greatly increase.

In Figure 9, we display the influence of the transpiration parameter on the temperature distribution. As the flow is accelerated due to the increasing values of the transpiration parameter, the temperature profiles are greatly increased.

Figure 10 displays the effects of the thermal buoyancy parameter on the temperature profiles. It is observed that an increase in thermal and solutal Grashof number causes a decrease in the thermal boundary layer thickness, and consequently the fluid temperature decreases due to buoyancy effect. Physically, when λ_1/λ_2 (*i.e.*, the buoyancy effect) increases, the convection cooling effect increases and hence the fluid flow accelerates. Therefore both the temperature and the concentration reduce.

Figure 11 illustrates the effect of increasing the Prandtl number on the temperature profiles. It can be clearly seen on this figure that increases in Pr bring about a significant decrease in the fluid temperature. This is expected because the thermal boundary becomes thinner for larger values of the Prandtl number. Therefore, with an increase in the Prandtl number, the rate of thermal diffusion drops.

The effects of thermal radiation on the temperature profiles in the boundary layer are illustrated in Figure 12. We observe in this figure that increasing thermal radiation param-

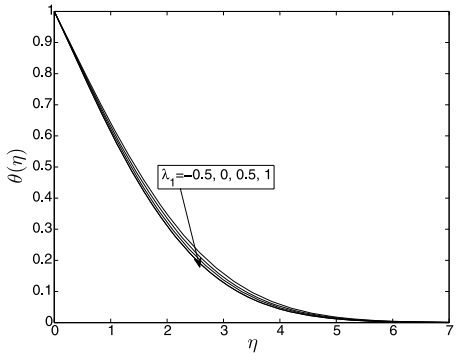

Figure 10 Graph of the SLLM solutions of the temperature profiles for different values of λ_1, with $\lambda = 0.5$; $R = 1$; $Pr = 0.71$; $\lambda_1 = 0.5$; $\lambda_2 = 0.5$; $Ec = 0.1$; $\gamma = 0.1$; $M = 0.5$; $\delta = 0.1$; $Sc = 0.22$.

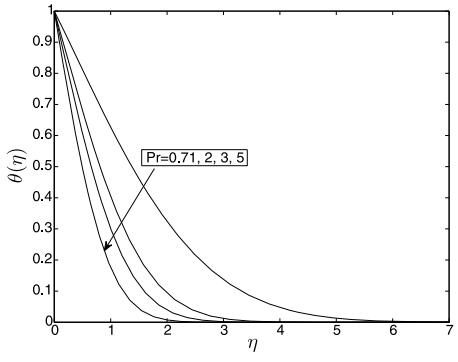

Figure 11 Graph of the SLLM solutions of the temperature profiles for different values of Pr, with $\lambda = 0.5$; $R = 1$; $\lambda_1 = 0.5$; $\lambda_2 = 0.5$; $Ec = 0.1$; $\gamma = 0.1$; $M = 0.5$; $\delta = 0.1$; $Sc = 0.22$.

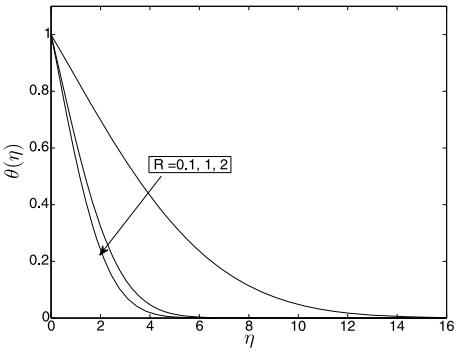

Figure 12 Graph of the SLLM solutions of the temperature profiles for different values of R, with $\lambda = 0.5$; $R = 1$; $Pr = 0.71$; $\lambda_1 = 0.5$; $\lambda_2 = 0.5$; $Ec = 0.1$; $\gamma = 0.1$; $M = 0.5$; $\delta = 0.1$; $Sc = 0.22$.

eter produces a significant decrease in the thermal condition of the fluid flow. This can be explained by the fact that a decrease in the values of R means a decrease in the Rosseland radiation absorptivity $k1$. Thus the divergence of the radiative heat flux decreases as k_1 increases the rate of radiative heat transferred from the fluid and consequently the fluid temperature decreases.

Figure 13 shows the effect of the chemical reaction parameter on the concentration; physically, as the chemical reaction parameter increases, the concentration profiles decrease, as can be clearly observed on this figure.

In Figure 14, we display the influence of the unsteadiness parameter $\lambda 1$ in the concentration profiles. Increasing the values of this parameter enhances the solutal boundary layer, thereby increasing the concentration distribution within the fluid flow.

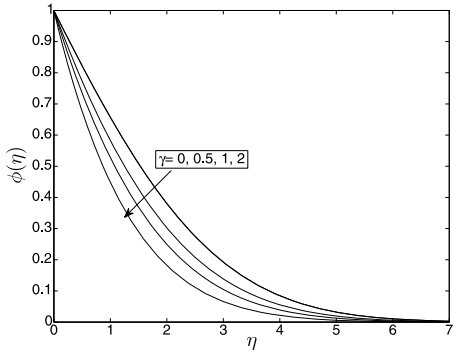

Figure 13 Graph of the SLLM solutions of the concentration profiles for different values of γ, with $\lambda = 0.5$; $R = 1$; $Pr = 0.71$; $\lambda_1 = 0.5$; $\lambda_2 = 0.5$; $Ec = 0.1$; $R = 1$; $M = 0.5$; $\delta = 0.1$; $Sc = 0.22$.

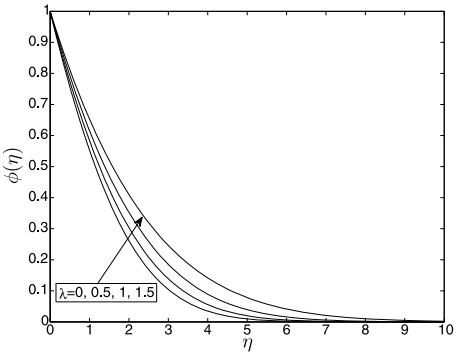

Figure 14 The influence of the unsteadiness number on the concentration distribution with $Ec = 0.1$; $R = 1$; $Pr = 0.71$; $\lambda_1 = 0.5$; $\lambda_2 = 0.5$; $Ec = 0.1$; $\delta = 0.1$; $M = 0.5$; $\delta = 0.1$; $Sc = 0.22$; $\gamma = 0.1$.

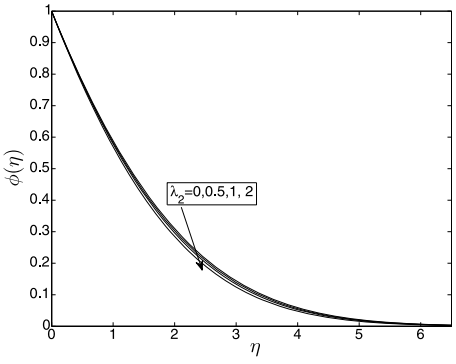

Figure 15 The influence of the concentration buoyancy number on the concentration distribution with $Ec = 0.1$; $R = 1$; $Pr = 0.71$; $\lambda_1 = 0.5$; $\lambda = 0.5$; $Ec = 0.1$; $\delta = 0.1$; $M = 0.5$; $\delta = 0.1$; $Sc = 0.22$.

Figure 15 depicts the influence of the solutal buoyancy on the concentration profiles. The buoyancy effect slightly reduces the concentration profiles.

Lastly, Figure 16 displays the effect of the Schmidt number on the concentration profiles. We observe that an increase in the Schmidt number (Sc) decreases the concentration boundary layer thickness. The Schmidt number represents the relative ease of the occurrence of the molecular momentum and the mass transfer and is very important in calculations of the binary mass transfer in multiphase flows.

6 Conclusion

The problem of unsteady MHD flow was studied near a stagnation point of a two-dimensional porous body with heat and mass transfer, thermal radiation, and chemical reaction. The partial differential governing equations were developed and transformed

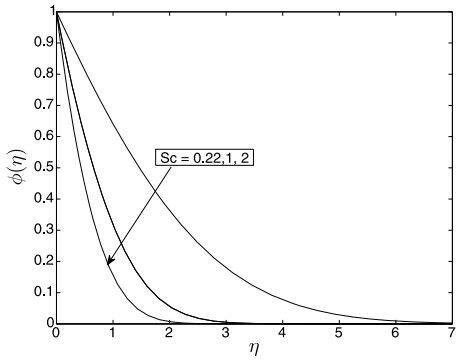

Figure 16 Graph of the SLLM solutions of the concentration profiles for different values of *Sc*, with $\lambda = 0.5$; $R = 1$; $Pr = 0.71$; $\lambda_1 = 0.5$; $\lambda_2 = 0.5$; $Ec = 0.1$; $R = 1$; $M = 0.5$; $\delta = 0.1$; $\gamma = 0.1$.

into a similar form by applying suitable similarity transformations. The similarity equations were solved numerically using the spectral local linearization method together with the successive relaxation method. From the numerical results, it is observed that:

1. Increasing the values of the magnetic field parameter resulted in increases in the skin-friction coefficients, whereas the Nusselt number and the Sherwood number and the velocity profiles decrease with increasing values of the magnetic parameter.
2. The skin-friction coefficient, the Nusselt number, and the Sherwood number increase with fluid injection.
3. The skin-friction coefficients also increase with increasing values of the heat source, the unsteadiness parameter, and the buoyancy parameters as well as the Eckert number.
4. The presence of a heat source has significant effects on the Nusselt number as well as on the temperature distribution in the fluid flow.
5. The thermal and solutal boundary layer thicknesses increase with increasing values of the unsteadiness parameter and Eckert number but decrease with increasing values of the buoyancy parameters.

Competing interests
The authors declare that they have no competing interests.

Authors' contributions
SS formulated, generated and discussed the results and GTM generated the code, discussed the results and proof read the manuscript.

Greek letters

β	thermal expansion coefficient
β_c	compositional expansion coefficient
η	similarity variable
σ	electrical conductivity
λ	unsteadiness parameter
λ_1, λ_2	buoyancy parameters
μ	coefficient of viscosity
ν	kinematic viscosity
θ	dimensionless temperature
ϕ	dimensionless concentration

Nomenclature

a, b	velocity gradient parameters at the boundary layer edge in the x- and y-directions
B_O	magnetic induction
C_f	skin-friction coefficient
c_p	heat capacity at constant pressure
Ec	Eckert number
D	mass diffusion
g	gravitational acceleration
f	dimensionless stream function
k_c	chemical reaction parameter
k	thermal conductivity coefficient
M	Hartmann number
Pr	Prandtl number
R	thermal radiation parameter
Q_0	heat generation/absorption coefficient
Re_l	Reynolds number
Sc	Schmidt number
T	temperature
t	dimensional time
u_e	dimensional free stream velocity component in x-direction
(u, v)	velocity components
(x, y)	transverse and normal directions

Author details

[1]Department of Mathematics, University of Venda, P Bag X5050, Thohoyandou, 0950, South Africa. [2]Department of Mathematics, University of Swaziland, Private Bag 4, Kwaluseni, Swaziland, South Africa.

Acknowledgements

The authors wish to acknowledge financial support from the University of Venda and NRF. The authors are very grateful to the reviewers for their constructive suggestions.

Received: 18 August 2014 Accepted: 12 September 2014 Published online: 02 October 2014

References

1. Hiemenz, K: Die Grenzschicht in Einem in Dem Gleichformingen Flussigkeitsstrom Eingetauchten Gerade Kreiszlinder. Dinglers Polytech. J. **326**, 321-410 (1911)
2. Wang, CY: Stagnation flow towards a shrinking sheet. Int. J. Non-Linear Mech. **43**, 377-382 (2008)
3. Motsa, SS, Khan, Y, Shateyi, S: A new numerical solution of Maxwell fluid over a shrinking sheet in the region of a stagnation point. Math. Probl. Eng. (2012). doi:10.1155/2012/290615
4. Shateyi, S, Makinde, OD: Hydromagnetic stagnation point flow towards a radially stretching convectively heated disk. Math. Probl. Eng. (2013). doi:10.1155/2013/616947
5. Chamkha, AJ, Ahmed, SE: Unsteady MHD heat and mass transfer by mixed convection flow in the forward stagnation region of a rotating sphere in the presence of chemical reaction and heat source. In: Proceedings of the World Congress on Engineering, WCE, July 6-8, vol. I (2011)
6. Bararnia, H, Ghotbi, AR, Domairry, G: On the analytical solution for MHD natural convection flow and heat generation fluid in porous medium. Commun. Nonlinear Sci. Numer. Simul. **14**, 2689-2701 (2009)
7. Pal, D, Talukdar, B: Combined effects of Joule heating and chemical reaction on unsteady magnetohydrodynamic mixed convection of a viscous dissipation fluid over a vertical plate in a porous medium with thermal radiation. Math. Comput. Model. **54**, 3016-3036 (2011)
8. Hayat, T, Awais, M, Safdar, A, Hendi, AA: Unsteady three dimensional flow of couple stress fluid over a stretching surface with chemical. Nonlinear Anal., Model. Control **17**(1), 47-59 (2012)
9. Najib, N, Bachok, N, Arifin, NM, Ish, A: Stagnation point flow and mass transfer with chemical reaction past a stretching/shrinking cylinder. Sci. Rep. **4**, 4178 (2014). doi:10.1038/srep04178
10. Patil, PM, Anilkumar, D, Roy, S: Unsteady thermal radiation mixed convection flow from a moving a vertical plate in a parallel free stream: effect of Newtonian heating. Int. J. Heat Mass Transf. **62**, 534-540 (2013)
11. Admon, MA, Kasim, ARM, Shafie, S: Unsteady free convection flow over a three-dimensional stagnation point with internal heat generation or absorption. World Acad. Sci., Eng. Technol. **51**, 530-535 (2011)
12. Ahmad, K, Nazar, R: Unsteady magnetohydrodynamic mixed convection stagnation point flow of a viscoelastic fluid on a vertical surface. J. Qual. Meas. Anal. **6**(2), 105-117 (2010)
13. Chamkha, AJ, Ahmed, SE: Similarity solution for unsteady MHD flow near a stagnation point of a three-dimensional porous body with heat and mass transfer, heat generation/absorption and chemical reaction. J. Appl. Fluid Mech. **4(2)**(1), 87-94 (2011)
14. Mahmoud, MAA: Thermal radiation effects on MHD flow of a micropolar fluid over a stretching surface with variable thermal conductivity. Physica A **375**, 401-410 (2007)
15. Rashidi, MM, Rostami, B, Freidoonimehr, N, Abbasbandy, S: Free Convective heat and mass transfer for MHD fluid flow over a permeable vertical stretching sheet in the presence of the radiation and buoyancy effects. Ain Shams Eng. J. (2014). doi:10.1016/j.asej.2014.02.007
16. Hassan, HN, Rashidi, MM: Analytical solution for three-dimensional steady flow of condensation film on inclined rotating disk by optimal homotopy analysis method. Walailak J. Sci. Technol. **10**, 479-498 (2013)
17. Basiri Parsa, A, Rashidi, MM, Anwar Bég, O, Sadri, SM: Semi-computational simulation of magneto-hemodynamic flow in a semi-porous channel using optimal homotopy and differential transform methods. Comput. Biol. Med. **43**(9), 1142-1153 (2013). doi:10.1016/j.compbiomed.2013.05.019. Epub2013 June 1

18. Khan, NA, Aziz, S, Khan, NA: Numerical simulation for unsteady MHD flow and heat transfer of a couple stress fluid over a rotating disk. PLoS ONE **9**(5), e95423 (2014). doi:10.1371/journal.pone.0095423
19. Eswara, AT, Nath, G: Effect of large injection rates on unsteady mixed convection flow at a three-dimensional stagnation point. Int. J. Non-Linear Mech. **34**, 85-103 (1999)
20. Trefethen, LN: Spectral Methods in MATLAB. SIAM, Philadelphia (2000)
21. Shateyi, S, Marewo, GT: A new numerical approach for the laminar boundary layer flow and heat transfer along a stretching cylinder embedded in a porous medium with variable thermal conductivity. J. Appl. Math. **2013**, Article ID 576453 (2013)
22. Shateyi, S, Marewo, GT: A new numerical approach of MHD flow with heat and mass transfer for the UCM fluid over a stretching surface in the presence of thermal radiation. Math. Probl. Eng. **2013**, Article ID 670205 (2013)

doi:10.1186/s13661-014-0218-z
Cite this article as: Shateyi and Marewo: **Numerical analysis of unsteady MHD flow near a stagnation point of a two-dimensional porous body with heat and mass transfer, thermal radiation, and chemical reaction.** *Boundary Value Problems* 2014 **2014**:218.